Experimental study on high-efficiency DC short electric arc milling of titanium alloy Ti6Al4V

Zongjie Zhou
Xinjiang University
Kai Liu
Xinjiang University
Yan Xu
Xinjiang University
Jianping Zhou (linkzhou@163.com)
Xinjiang University
Lizhong Wang (wanglz@mail.xjtu.edu.cn)
Xinjiang University

Research Article

Keywords: SEAM, Ti–6Al–4V, MRR, Moving arc

Posted Date: May 11th, 2021

DOI: https://doi.org/10.21203/rs.3.rs-357272/v1

Version of Record: A version of this preprint was published at The International Journal of Advanced Manufacturing Technology on August 17th, 2021. See the published version at https://doi.org/10.1007/s00170-021-07864-z.

Abstract

Short electric arc milling (SEAM) is an efficient electrical discharge machining method, especially for the efficient removal of difficult-to-machine conductive materials with high hardness, high toughness, and wear resistance. In this study, titanium alloy Ti–6Al–4V is used as the research object to conduct machining experiments. The material removal mechanism of SEAM technology is studied using a DC power supply and different tool electrode materials (copper, graphite, Q235 steel, and titanium). The energy distribution of the discharge gap is analyzed using a data acquisition system and a high-speed camera. The arc is found to move with the spindle rotation in the process of arc discharge, and multi-point discharge occurs in the process of single-arc discharge. The voltage and current waveforms and the radius of the etched particles during the experiment were counted, the material removal rate (MRR) and relative tool wear rate (RTWR) are calculated, and the surface and cross-section micromorphology and hardness are analyzed. The experimental results show that when the electrode material is graphite, the maximum feed rate is 650 mm/min, the MRR can reach 17268 mm^3/min, the ideal maximum MRR is more than 65000 mm^3/min, and the RTWR is only 1.27%. When the electrode material is Q235 steel, the minimum surface roughness is 35.04 μm, and this material has good stability under different input voltages. When the electrode material is copper, the hardness of the resolidified layer is close to that of the base material, which is beneficial for further processing. The lowest specific energy consumption is 18.26 kJ/cm^3 when titanium is used as the electrode material.

1. Introduction

Titanium alloy Ti–6Al–4V has good mechanical properties such as high strength, good corrosion resistance, and high heat resistance. It is widely used in the manufacturing of aircraft engine compressor parts and rockets, missiles, and high-speed aircraft structural parts, as reported by Shokrani et al. (2012) [1]. However, Dandekar et al. (2010) found that due to the low thermal conductivity of titanium alloy, it is difficult to expel the heat generated, resulting in extremely high temperatures in the cutting deformation area and a small range near the cutting edge, thus significantly shortening the tool life and resulting in a low processing efficiency and high cost [2]. Therefore, as an effective processing method for difficult-to-process conductive materials, electrical discharge machining (EDM) has been developed rapidly under the impetus of microelectronics, power electronics, and modern control technologies.

Reducing the tool loss and improving the material removal rate (MRR) have attracted the attention of many scholars. Fonda et al. (2008) studied the material removal mechanism and heat conduction characteristics of Ti6Al4V during EDM [3]. Li et al. (2020) proposed EDM-assisted milling to process Ti–6Al–4V alloys. The results show that compared with traditional milling, the electrode loss and cutting force are significantly reduced, and the surface quality is improved [4]. Kuriachen and Mathew (2015) established a transistor-type pulse discharge circuit model and proved that the capacitance has a significant impact on the EDM radius and can be used to predict the EDM radius in the machining of titanium alloys [5]. Yadav and Yadava (2015) studied the influences of the electrical parameters and rotation speed on the dimensional accuracy and surface quality of titanium alloys during EDM drilling; a

rotating electrode was found to have the most significant impact on the results [6]. Zhao et al. (2015) proposed blasting erosion processing using multi-hole electrodes, which significantly improved the processing efficiency [7]. Han et al. (2009) found that the electrode loss can be effectively reduced in conventional EDM under oil dielectric conditions [8]. Although the above research on EDM technology makes the machining performance of titanium alloys better than that of traditional machining in terms of the tool loss, surface quality, and dimensional accuracy, it is insufficient for applications requiring mass removal of materials. Short electric arc machining (SEAM) technology has significant advantages in this regard.

The SEAM proposed by Zhou et al. (2008) is a type of machining method that uses instantaneous high temperatures generated by a short arc discharge between electrodes to remove conductive metals under the action of a certain proportion of gas–liquid mixture medium at a certain pressure. It uses low voltage and high current source to generate continuous arc in a water–air mixture medium or air to quickly remove conductive metal materials [9]. Wang et al. (2014) proposed a high-speed EDM and arc hybrid machining method with DC voltage and pulse voltage in parallel, which significantly improved the MRR under the condition that the electrode loss is similar to that of conventional EDM [10]. Zhu et al. (2016) used a high-frequency (500 Hz), high-voltage power (1000 V) parallel DC power supply and found that, the higher the pulse voltage, the higher the MRR and the lower the tool wear rate (TWR) [11]. Shen et al. (2015) used a high-frequency pulse voltage (310 V/5 kHz) and a low-frequency pulse voltage (70 V/80 Hz) parallel hybrid power supply for EDM milling, realizing improved machining stability and MRR [12]. Kou and Han (2018) proposed a moving arc high-speed EDM milling method to process titanium alloys, studied the arc elimination mechanism and process, and obtained high MRR and low electrode loss [13]. Liu et al. (2020) studied the effect of electrode polarity on DC short arc milling of titanium alloys and found that electrode negative machining can yield a higher machining efficiency [14]. Li et al. (2018) studied the influence of different electrode materials on pulse short arc milling and found that graphite provides a lower electrode loss rate, whereas red copper provides better surface quality [15]. Chen et al. (2019) studied short arc milling GH4169 with a pulse power supply and further revealed the material removal mechanism by analyzing the influence of process parameters and electrode polarity changes on machining performance [16]. In summary, SEAM has shown excellent performance in machining shaft parts made of difficult-to-machine materials. It inherits the advantages of the EDM while being cost-effective and highly efficient.

In this study, the DC SEAM method is used to analyze the influence of different electrode materials on titanium alloy Ti–6Al–4V. With the help of a high-speed camera, the formation process, discharge characteristics, and erosion mechanism of DC arc are explored, which lays a theoretical foundation for the further development of SEAM.

2. Experiment Details

2.1 Experimental principle

SEAM is a partial non-equilibrium thermodynamic process under the coupling effect of multiple physical fields. Its essence is to form electric arc discharge in a short distance channel by inducing a voltage breakdown between the tool electrode and workpiece. The high-density heat energy generated in the arc channel melts the parts to be machined, and the melt is eroded under the combined action of the blowing force of the high-pressure airflow and the thermal explosion force. The processing schematic of SEAM is shown in Fig. 1, mainly including CNC machine tools, power supplies, air compressors, water circulation systems, data acquisition systems, and high-speed camera systems.

As shown in Fig. 2(a), as the gap between the electrodes decreases, the electric field strength between the electrodes increases sharply during operation. Under the electric field, the gas–liquid-mixed medium containing a certain number of conductive particles (such as fine metal particles, conductive particles in liquids) will also play a “bridging” role under the electric field strength, thereby making the electrons and conductive ions between the electrodes to move toward the two poles under the electric field. When the electrons move toward the anode at high speeds, they collide with the molecules or neutral atoms in the two-phase water–gas-mixed medium, resulting in collision ionization, forming more negatively charged electrons and positively charged ions, resulting in avalanche surge of the charged particles, which produces extremely high temperatures in a few microseconds. Under the action of high-temperature gasification, a melting zone and a heat-affected zone are formed around the arc. The high-density heat energy generated in the arc channel melts the part to be machined, and the melt is taken away from the discharge area under the combined action of the high-pressure air blowing force and thermal explosion force. Figure 2(b) shows the short arc field processing image.

2.2 Experimental conditions

The experimental equipment includes:

1. Experimental equipment: Short electric arc CNC milling machine, high power pulse power supply, metallographic microscope, metallographic sample grinding machine, and polishing machine.

2. Workpiece material: Ti–6Al–4V; its mechanical properties are listed in Table 1.

3. Tool electrode: Copper, graphite, Q235 steel, and Ti tubular electrode with an inner diameter of 6 mm and an outer diameter of 18 mm; the electrode speed is 600 r/min. Table 2 lists the thermophysical properties of the electrode and workpiece materials at room temperature.

4. Testing equipment: Precision balance with an accuracy of 0.1 mg, DeweSoft SIRIUSi multichannel data acquisition system, microhardness tester (HXD-100tb), scanning electron microscope (MERLIN Compact), and super-depth field microscope (VHX-6000).

Table 1
Mechanical properties of Ti–6Al–4V.

Microhardness	Elastic Modulus	Tensile strength	Yield strength	Elongation	Density
370–430 HV	1.012Gpa	1070 MPa	970 MPa	15%	4.51g/cm^3

Table 2
Thermophysical properties of electrode and workpiece materials at room temperature.

Thermal physical constants	Copper	Graphite	Q235 steel	Ti	Ti-6Al-4V
Melting point (℃)	1083	3652	1495	1668	1678
Boiling point (℃)	2567	4830	2735	3287	3280
Thermal conductivity (W/m·℃)	386	129	52.34	12.56	7.96
Heat capacity (J/Kg·℃)	394	710	502	578	612

2.3 Experimental setup

To explore the influence of different electrode materials on the SEAM of titanium alloy Ti–6Al–4V, experiments were carried out with different input voltages as variables in this study. The detailed parameters of the experiment scheme are shown in Table 3. By extracting the peak current (I_P), single-arc discharge time, MRR, RTWR, and other data, the surface morphology, cross-section morphology, chemical composition, and microhardness of the workpiece were studied. The parameters of the single-arc discharge experiment scheme of the different electrode materials are shown in Table 4. The energy and current dynamic change mechanism of a single arc of a graphite electrode material were studied using a high-speed camera and data acquisition system.

Table 3
Parameter settings of SEAM

Parameter	Value
Tool polarity	Negative
Open voltage (V)	15, 20, 25, 30
Air pressure (MPa)	0.3
Flow rate (L/min)	5
Depth of machining (mm)	4
Tool speed (r/min)	600

Table 4
Parameter settings of single-arc

Parameter	Value
Tool polarity	Negative
Open voltage (V)	30
Air pressure (MPa)	0.3
Flow rate (L/min)	5
Tool speed (r/min)	1200
High-speed camera (fps)	1000

The calculation formulae for the MRR, RTWR, and SEC are as follows:

$$MRR = \frac{1000(M_{wi} - M_{wj})}{\rho_w t} \times 100\% \quad (1)$$

$$Ideal\ MRR = W \times D \times V_m\ (mm^3/\text{min}) \quad (2)$$

$$TWR = \frac{M_{ei} - M_{ej}}{M_{wi} - M_{wj}} \times 100\% \quad (3)$$

$$SEC = \frac{\rho_w \cdot \int_0^t (V \times I)dt}{(M_{wi} - M_{wj})}\ (\text{kJ/cm}^3) \quad (4)$$

where M_{wi} and M_{wj} denote the masses (g) of the workpiece before and after processing, respectively, ρ_w denotes the density of the workpiece (g/cm^3), t is the processing time (min), M_{ei} and M_{ej} denote the masses (g) of the tool before and after machining (g), respectively, V refers to the output voltage (V) of the power supply during machining, I refers to the current (A) through the gap, W refers to the actual milling width, D refers to the actual milling depth, and V_m is the maximum feed speed. The SEC is the specific energy consumed to remove a unit volume of material.

3. Results And Discussion

3.1 Material removal rate and relative tool wear rate

Figure 3 shows the effect of voltage variation on the MRR of different electrodes. The MRR has little difference when the voltage is low. The reason for this phenomenon is that the energy generated by the arc is limited, and the processing speed is low under the condition of low voltage. With the increase in the voltage, the MRR of the four electrode materials increases to varying degrees. The MRR of the graphite

electrode has the most significant increasing trend. The MRRs of copper and graphite are similar, whereas that of titanium is the lowest. When the voltage is 30 V, the maximum feed rate of the graphite electrode can reach 650 mm/min. According to formula (1), the actual MRR is 17268 mm^3/min. This is due to the lower feed speed in the initial stage of processing, which increases the overall processing time. According to formula (2), the MRR can exceed 65000 mm^3/min if the electrode loss is neglected. The removal rates of copper, Q235 steel, and titanium were 6287, 5709, and 2803 mm^3/min, respectively, at 30 V, mainly due to the loss of electrode material.

Figure 4 shows the influence of different voltages on the RTWRs of different electrode materials. As shown in the figure, the RTWR of the four electrode materials decreases with the increase in the voltage. The upper left corner of Fig. 4 shows the processed images of the electrode materials under a voltage of 30 V. The RTWR of graphite electrode is the lowest, and the relative electrode loss is only 1.27% at a voltage of 30 V. This is mainly due to the higher melting point and heat capacity of graphite. The RTWRs of copper and Q235 steel are 40.44% and 47.5% respectively, and the losses are at the corners. This is because their melting and boiling points are low, and the position of discharge center on the electrode surface is easily melted and vaporized during the processing. The RTWR of titanium is 104.29%, and the loss is mainly at the end face. This is largely due to the poor thermal conductivity of titanium, which easily leads to the melting of the electrode material at continuously high temperatures during the processing. Therefore, when titanium is used as the electrode material, an axial tool compensation is required.

3.2 Specific energy consumption

Through a statistical analysis of the electrical parameters obtained from the data acquisition system, the influence of voltage on the SEC of different electrode materials is shown in Fig. 5. The SEC of the different electrode materials gradually decreases with the increase in the voltage. When the voltage is 15 V, the SEC is highest for graphite, 756.2 kJ/cm^3. This is mainly due to the lower conductivity of graphite compared with those of the other three materials, which leads to greater energy consumption. With the increase in the voltage, the increased material removal leads to a significant reduction in the energy consumption. When the voltage is 30 V, the energy consumptions of copper and Q235 steel are 107.16 kJ/cm^3 and 84.85 kJ/cm^3 respectively. The main reason is that the material removal is reduced due to excessive electrode loss. The energy consumption of titanium is the lowest and changes little with increasing voltage; it is only 18.26 kJ/cm^3 at 30 V. This phenomenon is mainly due to the low thermal conductivity of titanium, which easily leads to an increase in the temperature of the processing area and helps remove material. Compared with the other electrode materials, the voltage has little effect on the energy consumption of titanium electrode.

3.3 Surface roughness

The influence of voltage on the SR of the workpiece processed with different materials is shown in Fig. 6. In this study, the SR was expressed using the parameter *Sa* (arithmetic mean height of the surface). The *Sa* values of graphite and titanium electrode materials increase significantly with the increase in the

voltage, whereas the increase is minor in the case of copper and Q235 steel electrode materials. When the voltage is 15 V, the *Sa* values of graphite, titanium, copper, and Q235 steel electrodes are 21.58, 30.59, 38.75, and 32.71 μm, respectively. This is because when the voltage is low, the arc energy is limited, and the processing speed is low. The melted material in the processing area can be discharged in time with the rotation of the electrode and the erosion of the working medium; hence, *Sa* is low. With the increase in the voltage, due to the difference in the conductivity and other thermophysical properties of the different electrode materials, the volume of the melted material in the processing area will increase to varying degrees with the increase in the arc energy, which causes the surface roughness of the workpiece to change to varying degrees.

3.4 Analysis of single-arc discharge

To explore the single-arc discharge energy difference and current dynamic change mechanism of the different electrode materials, the data are statistically analyzed using a data acquisition system and a high-speed camera. The experimental results of the single-arc discharge at 30 V are shown in Fig. 7. Figure 7(a) shows the machining traces formed by single-arc discharge of the different electrode materials on the Ti–6Al–4V surface. The graphite electrode has the highest discharge energy, with the pit diameter reaching 23.99 mm, followed by copper and Q235 steel, with pit diameters of 23.28 mm and 23.03 mm, respectively. The discharge energy is lowest for the titanium electrode, and the pit diameter is 22.37 mm. Figure 7(b) shows the waveform corresponding to the single-arc discharge of the graphite electrode. The duration of a single-arc discharge is 123 ms, and the current waveform is unstable. Parts c, d and e in Fig. 7(b) are respectively the initial stage of the discharge channel establishment, the stage of current dynamic change, and the stage of current step change.

Figures 7(c), (d) and (e) show the arc dynamic change diagrams corresponding to the parts c, d, and e in Fig. 7(b), respectively. As the two poles comes closer, the electric field strength increases. Figure 7(c) shows that at 26.845 s, the voltage between the two poles breaks down the working medium, and an arc appears with a weak arc light. The current is very low at the initial stage of the establishment of the discharge channel, but then increases rapidly and reaches 800 A in approximately 10 ms. From the position shown in Fig. 7(c), we find that the position of the arc is shifted relative to the initial position with the rotation of the electrode, and it plays the role of breaking the arc under the high-speed rotation, which effectively avoids the electric discharge of the workpiece surface. This has important significance in the energy control of the arc. Figure 7(d) shows the arc state when the current rises steadily again under the original decreasing trend. Two arcs are generated in the discharge gap at 26.872 s, and they rotate along with the electrode. Combined with the current waveform shown in Fig. 7(b), the current begins to increase at the same time, which indicates that there are multiple discharge points in a single arc during the machining process. This will not end until all the discharge channels are extinguished at the same time, at which point the single-arc machining is complete. Figure 7(e) shows the corresponding arc state when the current changes step. From the corresponding current waveform shown in Fig. 7(b), the current decreases from the original trend and increases by 400 A instantaneously at 26.913 s. Figure 7(e) shows that the arc light is getting stronger, and even a flame is produced. This may be due to the short circuit at

the discharge point between the two poles, which causes the instantaneous current to increase. However, as the discharge point is eroded, the arc again tends to stabilize.

3.5 Analysis of voltage and current wave

Figure 8(a) shows the voltage and current waveforms of the copper electrode SEAM. The peak current (I_P) reaches 1109 A, and the corresponding single-arc discharge time is 59.23 ms. The discharge frequency is high, but the current is mostly low. This phenomenon is mainly due to the low heat capacity and melting point of copper and its high thermal conductivity. During the processing, secondary discharge or multiple discharges are induced due to the continuously melted particles on the electrode surface between the two poles. Figure 8(b) shows the voltage and current waveforms of graphite electrode SEAM, where the peak current (I_P) is 945 A, the corresponding single-arc discharge time is 48.79 ms, and the discharge frequency is the highest, which is almost continuous. This is mainly because the graphite electrode has the highest machining speed, low electrode loss, and the discharge channel between the electrode and the workpiece is established by high frequency. Figure 8(c) shows the voltage and current waveforms of the Q235 steel electrode SEAM; the peak current (I_P) is 1503 A, and the corresponding single-arc discharge time is 11.98 ms. The discharge frequency is low, and the single-discharge time is less, which is mainly due to the low melting point and thermal conductivity of Q235 steel. The high temperature of single-discharge energy leads to a large amount of material erosion. Figure 8(d) shows the voltage and current waveforms of the titanium electrode SEAM. The peak current (I_P) reaches 1181 A, and the corresponding single-arc discharge time is 8.87 ms. The discharge frequency is the lowest, and the single discharge time is the smallest. This is due to the low thermal conductivity of the electrode and the workpiece, the high temperature of the machining area makes the electrode and the workpiece melt simultaneously, and the discharge gap easily undergoes a short-circuit instantaneously, resulting in a significant leakage of the single-discharge energy.

3.6 Current proportional distribution

To study the energy distribution of the different electrode materials in the SEAM process of titanium alloy Ti–6Al–4V, the current in the machining process is statistically analyzed in intervals as shown in Fig. 9. In the SEAM of copper, graphite, Q235 steel, and titanium electrodes, the proportions of current in the range of 0–700 A are 98.22%, 95.1%, 87.9%, and 64.2% respectively, and the proportions of current in the range of > 700 A are 1.78%, 4.9%, 12.1% and 35.8% respectively. From the above data, it is evident that the energy intensities of the four electrode materials in EDM are different, which is mainly due to the electrical conductivity of the electrode materials and other external factors of SEAM. This is another important reason for the different energy consumptions.

3.7 Three-dimensional surface topography analysis

Figure 10(a) shows the 3D surface topography of the workpiece machined using the copper electrode when the voltage is 30 V. *Sa* and *Sz* are 52.05 μm and 619.75 μm, respectively, and the surface of the workpiece is relatively flat. This is due to the small energy of the single discharge and the fact that most of the discharge is small current discharge, and the surface pits formed in the machining process are

small. Figure 10(b) shows the 3D surface topography of the workpiece processed by the graphite electrode. *Sa* and *Sz* are 112.8 μm and 737.87 μm, respectively, and the surface quality of the workpiece is the worst. Due to the high processing speed, the rotation of the electrode, and the erosion of the working medium, the moving track of the workpiece after the arc erosion can be clearly seen. Figure 10(c) shows the 3D surface topography of the workpiece processed by the Q235 steel electrode. *Sa* and *Sz* are 35.04 μm and 359.61 μm, respectively. The surface quality of the workpiece is the highest, and there are evident traces of working medium scouring on the surface of the workpiece. Figure 10(d) shows the 3D surface topography of the workpiece processed by titanium electrode. *Sa* and *Sz* are 70.23 μm and 690.40 μm respectively, and the surface quality of the workpiece is poor. This is due to the low thermal conductivity and good elongation of the titanium electrode during the processing, and the material easily accumulates on the surface of the workpiece and solidifies again after melting at high temperatures.

3.8 Erosion particle radius

Figures 11 (a, b, c, d) show the erosion particles of the different electrode materials in the electric discharge gap of SEAM. Figure 11(e) shows the quantitative statistical analysis of the percentage data of different radii, realized through the image analysis software Engauge digitizer. Figures 11 (a, b, c, d) show that most of the particles produced by EDM of the four electrode materials are spherical, spherical shell or ellipsoidal, which indicates that the surface tension plays a major role in the phase transition of the particles from liquid to solid. The same was concluded by Xu et al. (2015) [17]. The statistical data in Fig. 11(e) show that the proportion distribution of particle radius is normal, as reported by Murti and Philip (1987) [18]. The particle radius produced by SEAM with the graphite electrode is the largest, with an average value of 574.7 μm, which is 30 times that produced by EDM. This is mainly due to the high energy density in the short arc milling process. The average radius of the particles produced by the SEAM of copper, Q235 steel, and titanium electrodes are 503.1, 402.5, and 279.9 μm, respectively. This result does not correspond to the energy density relationship of the different electrode materials, which indicates that particle formation is due to multiple factors.

3.9 Section profile dimensions

To study the influence of electrode loss on the machining dimension accuracy, the machining section is divided into an inlet section and an exit section based on the feed direction of the electrode, and the width is measured at the middle position of the machining depth. Figures 12 (a, b, c, d) show the cross-sectional dimension diagrams of copper, graphite, Q235 steel, and titanium electrode when the voltage is 30 V. The absolute differences in the two cross-sectional profile dimensions are 2603.7, 202.7, 2169.6, and 283.9 μm, respectively. The above data show that the cross-sectional dimension accuracy of graphite and titanium electrode materials is better, whereas the dimension deformations of copper and Q235 steel electrode are larger due to electrode loss in the processing.

3.10 Analysis of surface micromorphology

The surface micromorphologies of the workpiece processed with different electrode materials are shown in Figs. 13 (a, b, c, d). Evidently, there are different degrees of microcracks, spherical droplets, and

resolidified layer on the surface of the four types of electrode materials. Microcracks are formed when the corrosion products that cannot be discharged in time cover the surface of the workpiece under the rapid cooling of the working medium. and the concentrated stress due to the rapid change in the temperature exceeds the yield limit stress of the material. Spherical droplets fall on the recast layer due to the surface tension and gravity of the droplets in the molten pool. A resolidified layer is formed on the surface of the workpiece because the melted metal between the two poles is not discharged in time. Figures 13(e) and Fig. 13(f) show the EDS spectra of the droplets and resolidified layers formed on the surface of the workpiece processed using four types of electrode materials. The main elements in the droplets and recast layers are C, O, and Ti, and the corresponding metal elements of the electrode materials. This is mainly because at high temperatures, C, O, and Ti tend to undergo chemical reactions to form Ti oxides and carbides that attach onto the surface of the workpiece.

3.11 Analysis of workpiece section

Figures 14 (a, b, c, d) show the cross-sectional morphologies of Ti–6Al–4V workpieces processed by copper, graphite, Q235 steel, and titanium electrodes, respectively, and Figs. 14 (e, f, g, h) show the EDS spectra of the resolidified layer, heat-affected layer, and base material of the corresponding workpiece material. As shown in Fig. 14(a), the thickness of the heat-affected layer corresponding to copper is 44.5 μm, which is mainly due to the good thermal conductivity of copper, and most of the heat is dispersed in the discharge gap and electrode part. The maximum thickness of the heat-affected layer is for the workpiece material processed by the graphite electrode. As shown in Fig. 14(b), the maximum thickness reaches 162.6 μm, which is due to the high discharge frequency and high energy density during processing. As shown in Fig. 14 (c), the thickness of the heat-affected layer corresponding to Q235 steel is in the range of 55.2–80.4 μm, which is greater than that in the case of copper. This is due to the low heat conductivity of Q235 and slow cooling of the working fluid. As shown in Fig. 14(d), the thickness of the heat-affected layer corresponding to the titanium electrode is 38.6 μm; however, the resolidified layer is thicker and has many cracks. This is because the electrode and workpiece materials have extremely poor thermal conductivity; hence, a large amount of etchants easily accumulate on the surface of the workpiece. Most of the heat is distributed on the resolidified layer and cools rapidly with the working medium, resulting in a large number of microcracks.

Figures 14 (e, f, g, h) show that the main elements of the electrode material and working medium increase to different degrees in the resolidified layer and heat-affected layer of each workpiece. This is mainly because in the SEAM process of titanium alloy Ti–6Al–4V, the high temperature makes the electrode and workpiece to melt and vaporize in the working medium, and a complex chemical reaction occurs, which leads to the migration and penetration of the main elements in the electrode material and working medium to the resolidified layer or heat-affected layer. The amount of migration or penetration depth is determined by the loss of the electrode itself and the chemical reaction between the electric discharge gaps. Because the main elements of the titanium electrode are consistent with the workpiece material, it is conducive to the subsequent processing and treatment of the workpiece.

3.12 Section microhardness

The microhardness test of the workpiece section after SEAM processing with different electrode materials is shown in Fig. 15. In addition to the copper electrode, the microhardness of the other three electrode materials (graphite, Q235 steel, and titanium) increases significantly near the machined surface, and the maximum hardness values are 670, 887, and 717 HV, respectively. This position is mainly concentrated in the recast layer and part of the heat-affected layer, which is mainly due to the surface of the resolidified layer containing a large number of hard and brittle Ti oxides and carbides, as well as other metal elements. The maximum hardness of the workpiece section processed by the copper electrode is 348 HV, which is because the resolidified layer on the surface of the workpiece contains a large amount of copper, and its hardness is low, which is not significantly different from that of Ti–6Al–4V; hence, the hardness of this section hardly changes.

4. Conclusion

In this work, we mainly studied the material erosion mechanism of different electrode materials in the DC SEAM of titanium alloy Ti–6Al–4V and explored the influence of voltage on the processing with different electrode materials in terms of the MRR, RTWR, SEC, and SR. A single-arc discharge experiment was conducted to analyze the arc motion characteristics and the cause of the dynamic change in the current. The influences of the process characteristics in the DC SEAM of titanium alloy Ti–6Al–4V were comprehensively analyzed from many aspects. The main conclusions are as follows:

(1) The titanium alloy Ti–6Al–4V has the characteristics of high MRR and high energy density. When the voltage was 30 V, the maximum machining speed when using the graphite electrode was 650 mm/min, the MRR could reach 17268 mm^3/min, the ideal maximum MRR was more than 65000 mm^3/min, and the RTWR was only 1.27%.

(2) In the process of DC SEAM, the arc moves with the rotation of the electrode. In the process of single-arc discharge, multi-point discharges occurred simultaneously, which affected the trend in the current. An instantaneous short circuit between the electrodes led to a stepped change in the current.

(3) The heat-affected layer of the workpiece processed by the graphite electrode had the highest thickness (108.2–162.6 μm), the thicknesses of the heat-affected layer of the workpiece processed by the copper and Q235 steel electrodes were 44.5 μm and 80.4 μm, respectively, and the thickness of the heat-affected layer of the workpiece processed by the titanium electrode was the lowest (38.6 μm).

(4) In addition to the copper electrode, the hardness values of the other three electrode materials (graphite, Q235 steel, and titanium) increased significantly near the machined surface.

Declarations

Ethical Approval

Not applicable

Consent to Participate

Not applicable

Consent to Publish

Not applicable

Authors Contributions

Zhou Zongjie: Data curation, Writing-Original draft preparation. Liu Kai: Experimental planning, Data processing. Xu Yan: Investigation, Validation. Zhou Jianping: Conceptualization, Methodology. Wang Lizhong: Writing- Reviewing and Editing.

Funding

This research was supported by the Natural Science Foundation of China (Grant No. 51765063), the Key Research and Development Projects in the Autonomous Region (Grant No. 2018B02009-1), the Research and Innovation Project in the Autonomous Region (Grant No. XJ2019G032), and the Xinjiang University Doctoral Research and Innovation Project (Grant No. XJUBSCX-201908).

Competing Interests

The authors declare that they have no conflict of interest.

Availability of data and materials

All data generated or analysed during this study are included in this published article.

References

1. Shokrani A, Dhokia V, Newmann ST (2012) Environmentally conscious machining of difficult-to-machine materials with regard to cutting fluids. Int J Mach Tools Manuf 57:83–101. https://doi.org/10.1016/j.ijmachtools.2012.02.002
2. Dandekar C, Shin Y, Barnes J (2010) Machinability improvement of titanium alloy (Ti-6Al-4V) via LAM and hybrid machining. Int J Mach Tools Manuf 50:174–182. https://doi.org/10.1016/j.ijmachtools.2009.10.013
3. Fonda P, Wang Z, Yamazaki K, Akutsu Y (2008) A fundamental study on Ti-6Al-4V's thermal and electrical properties and their relation to EDM productivity. J Mater Process Technol 202(1–3):583–589. https://doi.org/10.1016/j.jmatprotec.2007.09.060
4. Li C, Xu M, Yu Z, Huang L, Li S, Li P, Niu Q, Ko T (2020) Electrical discharge-assisted milling for machining titanium alloy. J Mater Process Technol 285:116785-.

https://doi.org/10.1016/j.jmatprotec.2020.116785

5. Kuriachen B, Mathew J (2016) Spark radius modeling of resistance-capacitance pulse discharge in micro-electric discharge machining of Ti-6Al-4V: an experimental study. Int J Adv Manuf Technol 85(9–12):1983–1993. https://doi.org/10.1007/s00170-015-7999-9
6. Yadav U, Yadava V (2015) Experimental investigation on electrical discharge drilling of Ti-6Al-4V alloy. Mach Sci Technol 19(4):515–535. https://doi.org/10.1080/10910344.2015.1085316
7. Zhao W, Xu H, Gu L, Hong H, Rajurkar K (2015) Influence of polarity on the performance of blasting erosion arc machining. CIRP Ann Manuf Technol 64:213–216. https://doi.org/10.1016/j.cirp.2015.04.032
8. Han F, Wang Y, Zhou M (2009) High-speed EDM milling with moving electric arcs. Int J Mach Tools Manuf 49:20–24. https://doi.org/10.1016/j.ijmachtools.2008.08.005
9. Zhou J, Liang C, Teng W, Xu Y, Zhou B (2008) Study on rules in material removal rate and surface quality of short electric arc machining process. Adv Mater Res 33–37:1313–1318. https://doi.org/10.4028/www.scientific.net/AMR.33-37.1313
10. Wang F, Liu Y, Zhang Y, Tang Z, Ji R, Zheng C (2014) Compound machining of titanium alloy by super high speed EDM milling and arc machining. J Mater Process Technol 214:531–538. https://doi.org/10.1016/j.jmatprotec.2013.10.015
11. Zhu G, Zhang Q, Wang H, Wang K, Zhang M (2017) Machining behaviors of short electrical arc milling with high frequency and high voltage pulses. Int J Adv Manuf Technol 90:1067–1074. https://doi.org/10.1007/s00170-016-9399-1
12. Shen Y, Liu Y, Sun W, Dong H, Zhang Y, Wang X, Zheng C, Ji R (2015) High-speed dry compound machining of Ti6Al4V. J Mater Process Technol 224:200–207. https://doi.org/10.1016/j.jmatprotec.2015.05.012
13. Kou Z, Han F (2018) Machining characteristics and removal mechanisms of moving electric arcs in high-speed EDM milling. Journal of Manufacturing Processes 32:676–684. doi:10.1016/j.jmapro.2018.03.037
14. Liu K, Zhou J, Zhou Z, Xu Y, Hu G, Zhang L, Song D (2020) Milling performance of titanium alloy based on short electric arc machining with direct current power source. Int J Adv Manuf Technol 110:1641–1652. https://doi.org/10.1007/s00170-020-05937-z
15. Li XZ, Zhou JP, Wang KD, Xu Y, Wu TB (2019) Experimental research on machinability of different electrode materials for SEAM of the nickel-based superalloy GH4169. Proc Inst Mech Eng C J Mech Eng Sci 232(24): 4528–4537. https://doi.org/10/0954406218755184
16. Chen X, Zhou J, Wang K, Xu Y, Hu G (2019) A study on machining characteristics of nickel-based alloy with short electric arc milling. Int J Adv Manuf Technol 105(5–8):2935–2945. https://doi.org/10.1007/s00170-019-04501-8
17. Xu H, Gu L, Chen J, Hu J, Zhao W (2015) Machining characteristics of nickel-based alloy with positive polarity blasting erosion arc machining. Int J Adv Manuf Technol 79(5–8):937–947. https://doi.org/10.1007/s00170-015-6891-y

18. Murti V, Philip P (1987) An analysis of the debris in ultrasonic-assisted electrical discharge machining. Wear 117(2):241–250. doi:10.1016/0043-1648(87)90258-4

Figures

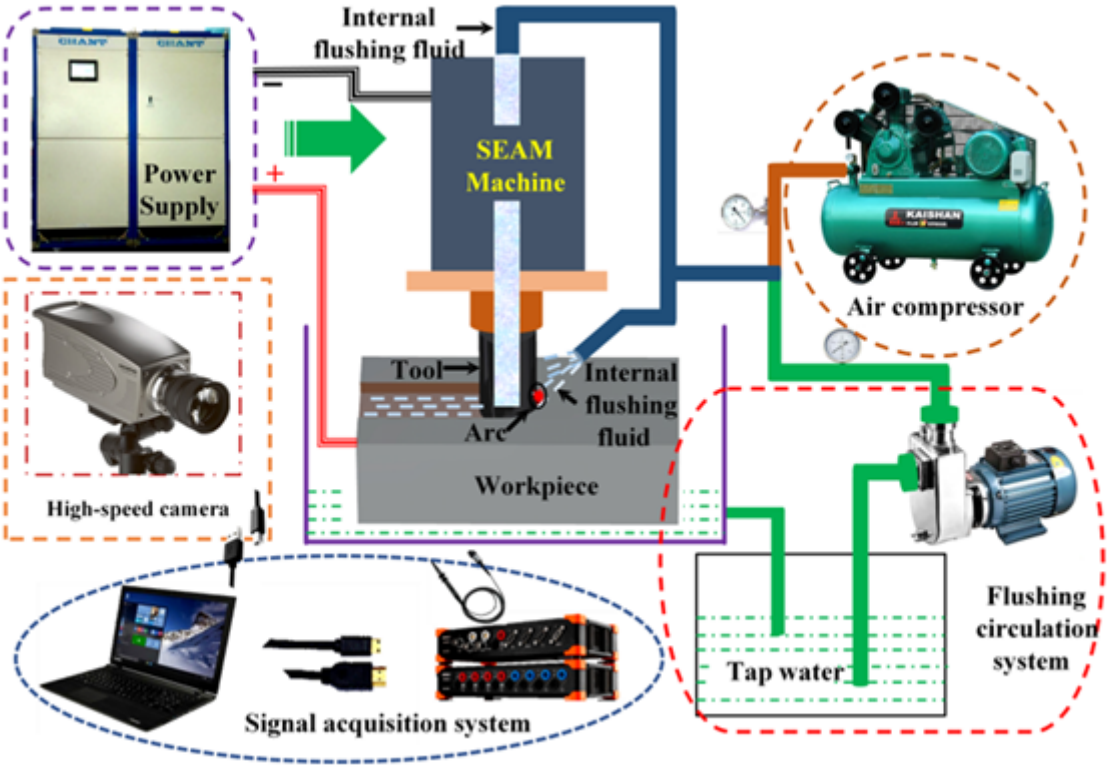

Figure 1

Schematic of SEAM.

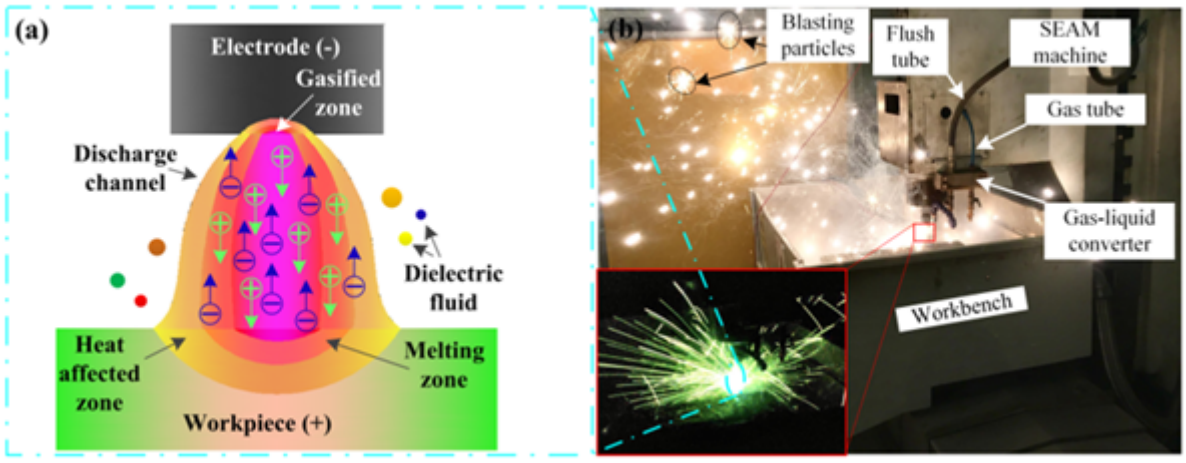

Figure 2

(a) Discharge channel model in SEAM, and (b) Image of the SEAM process.

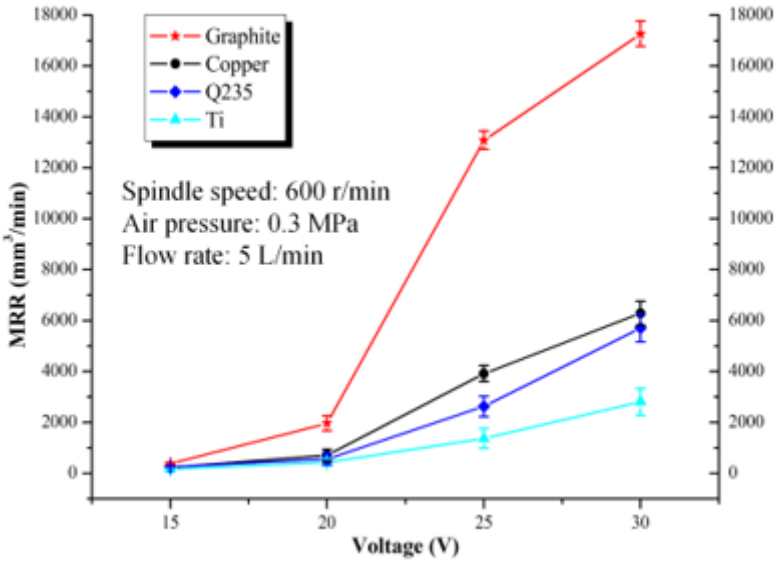

Figure 3

Material removal rate (MRR) of the workpiece

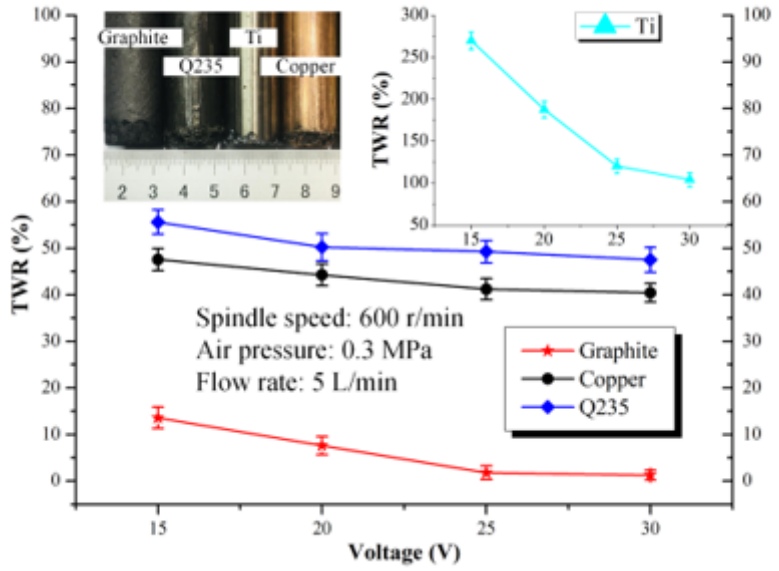

Figure 4

Relative tool wear rate (RTWR)

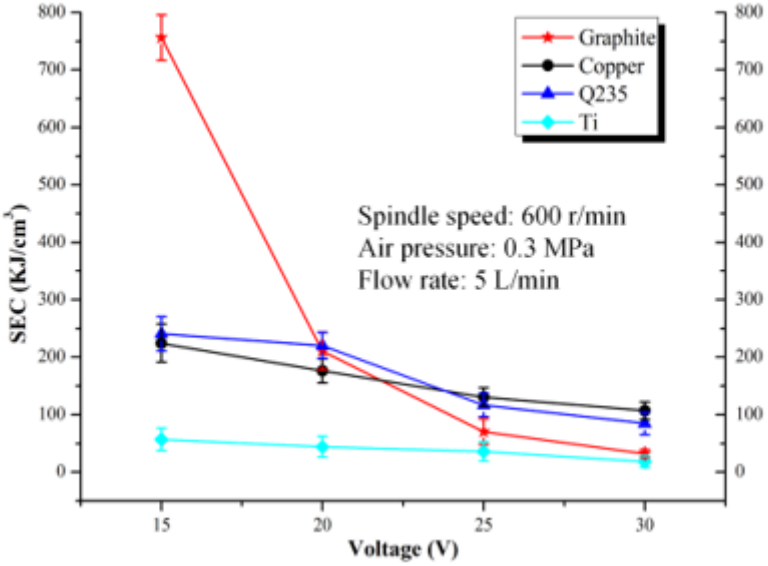

Figure 5

Specific energy consumption (SEC)

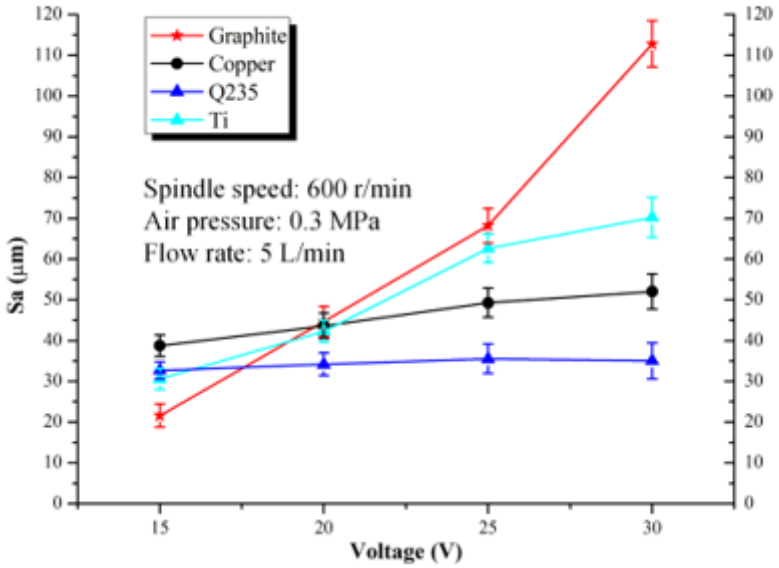

Figure 6

Surface roughness (SR)

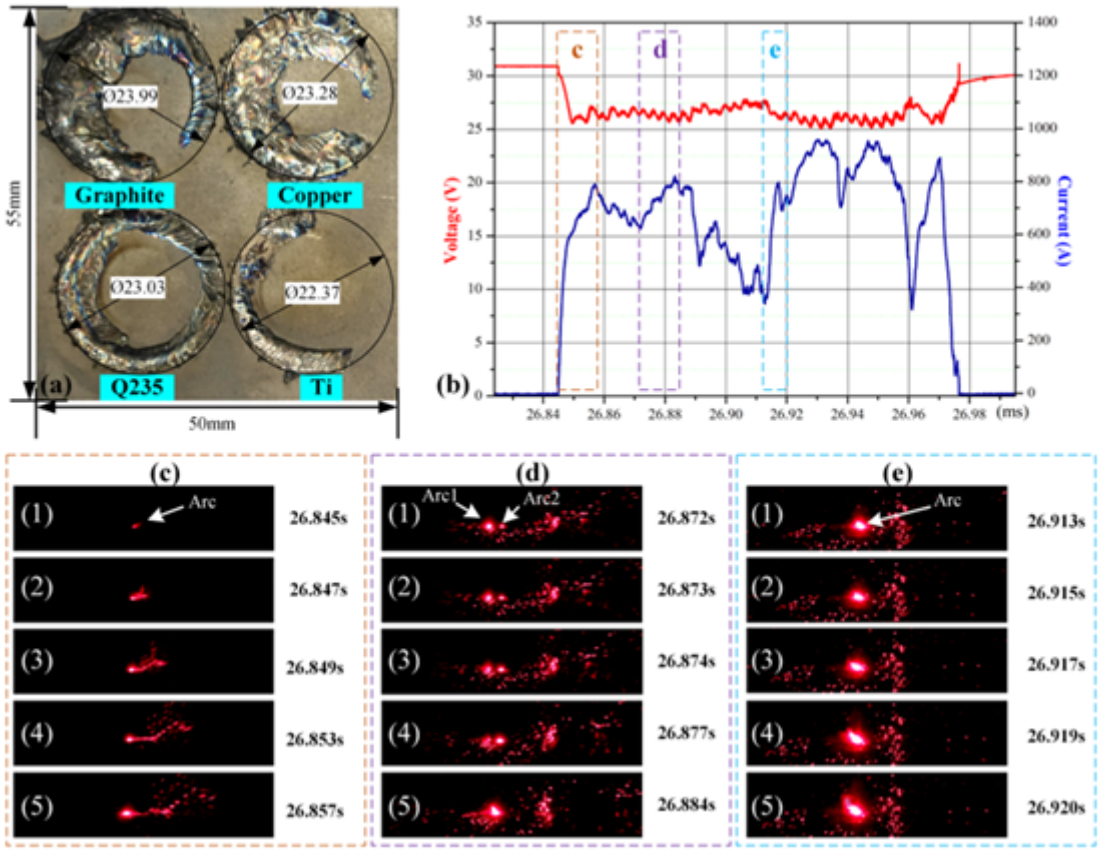

Figure 7

Single-arc discharge

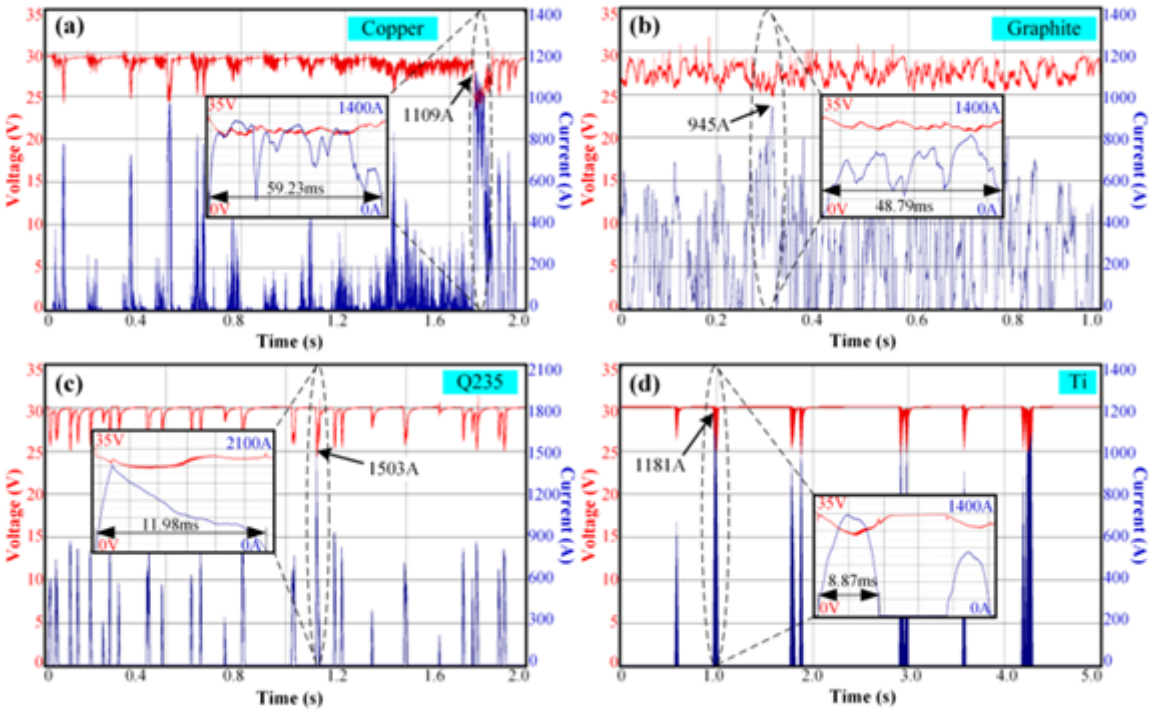

Figure 8

Output voltage and current waveforms in SEAM with different electrodes: (a) Copper, (b) Graphite, (c) Q235 steel, and (d) Ti.

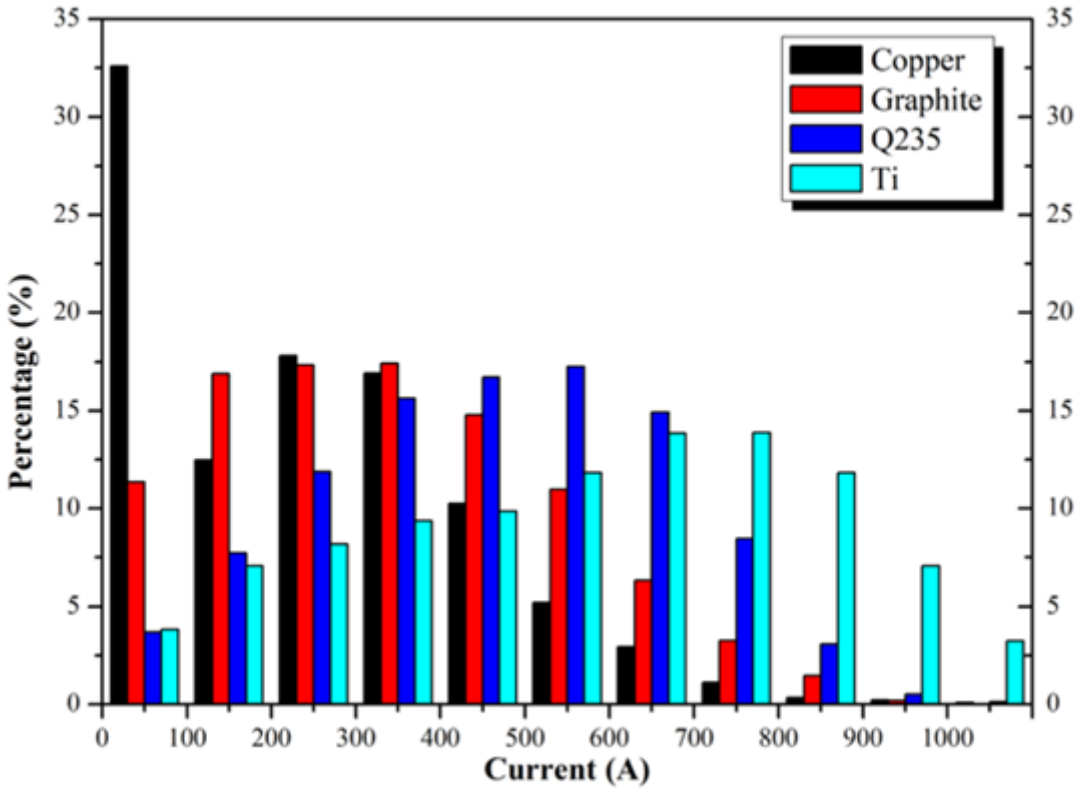

Figure 9

Current proportional distribution under different electrode SEAM

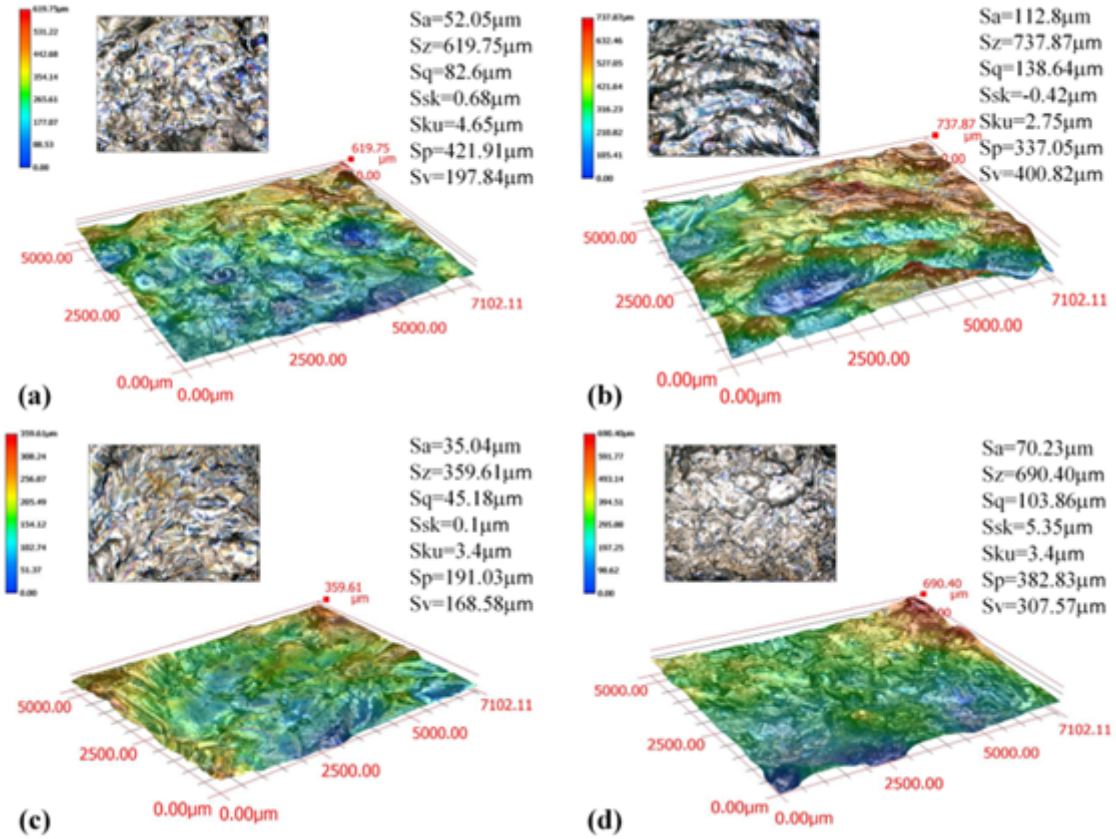

Figure 10

Three-dimensional surface topographies of workpieces processed under different electrodes in the SEAM process: (a) Copper, (b) Graphite, (c) Q235 steel, and (d) Ti.

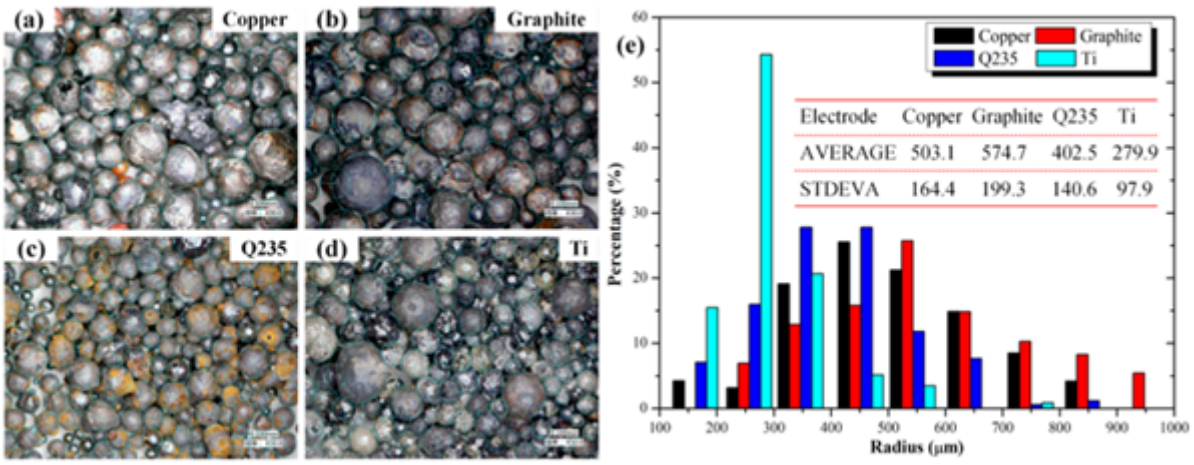

Figure 11

Erosion particle topographies of different electrodes prepared through SEAM. (a) Copper, (b) Graphite, (c) Q235 steel, (d) Ti, and (e) Percent distribution of particle radius.

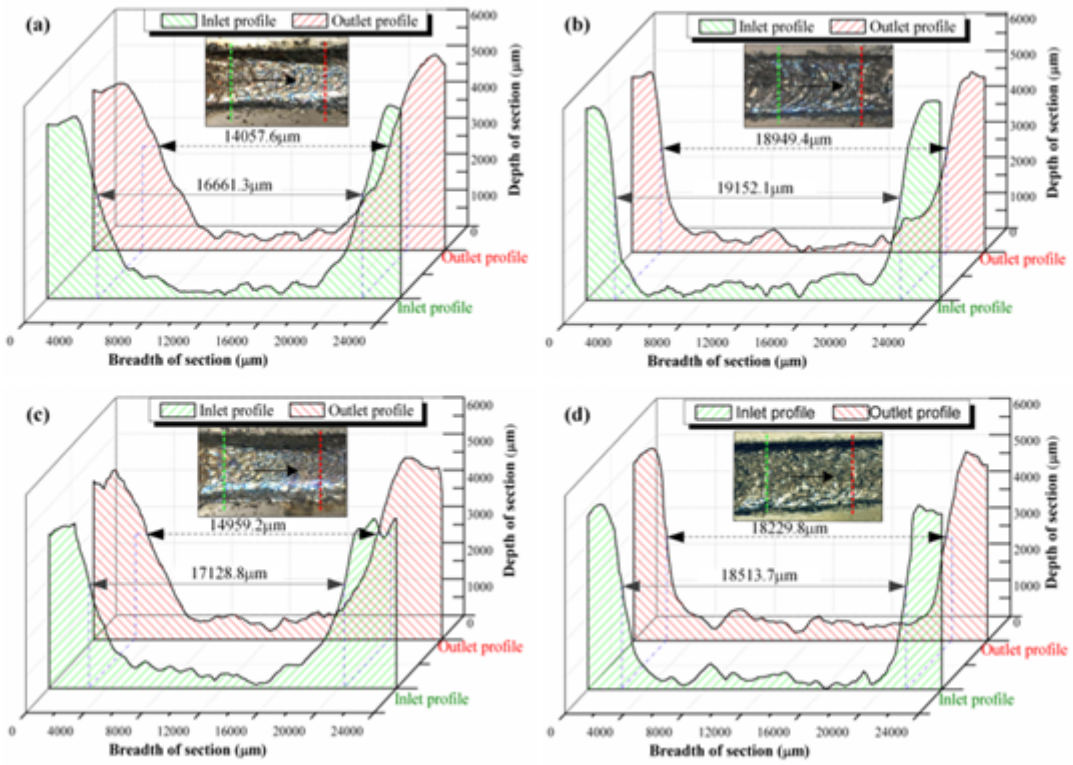

Figure 12

Section profile dimensions after SEAM with different electrodes. (a) Copper, (b) Graphite, (c) Q235 steel and (d) Ti.

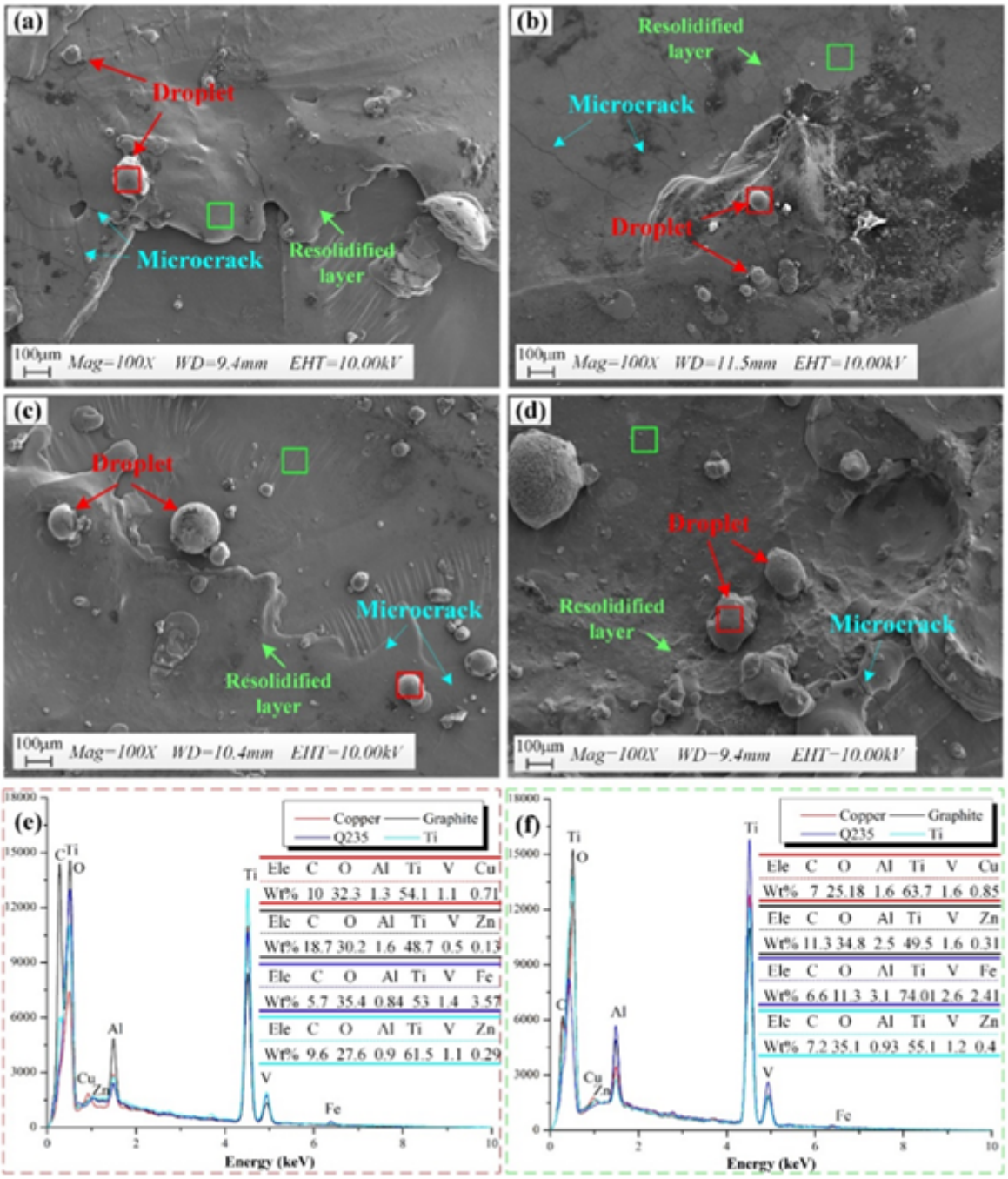

Figure 13

Micrographs of workpiece surface and EDS spectra under different electrode SEAM. (a) Copper, (b) Graphite, (c) Q235 steel, (d) Ti, (e) Droplet, and (f) Resolidified layer.

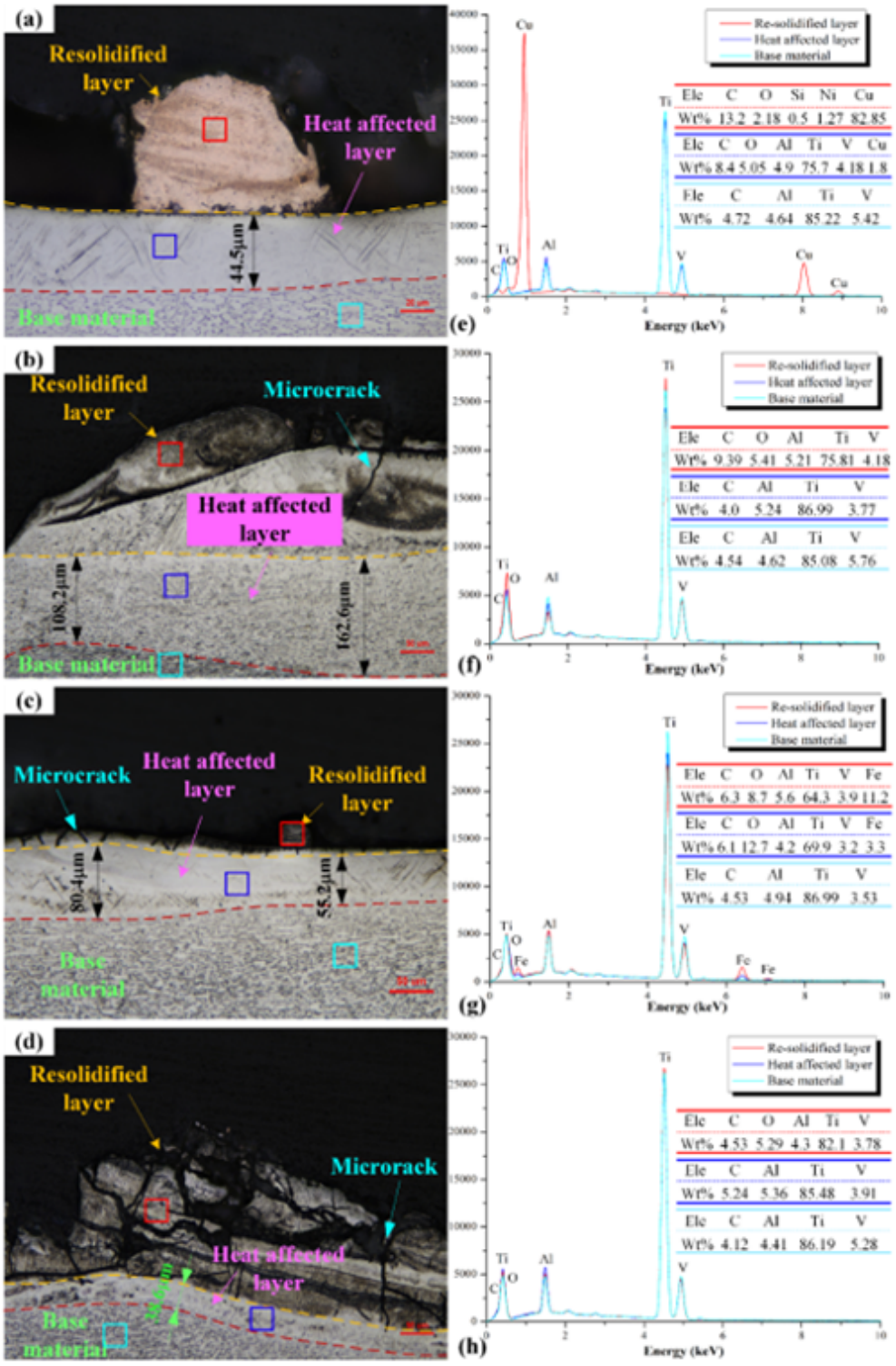

Figure 14

Micromorphologies of workpiece section and EDS spectra of workpieces processed using SEAM with different electrodes. (a, e) Copper, (b, f) Graphite, (c, g) Q235 steel, and (d, h) Ti.

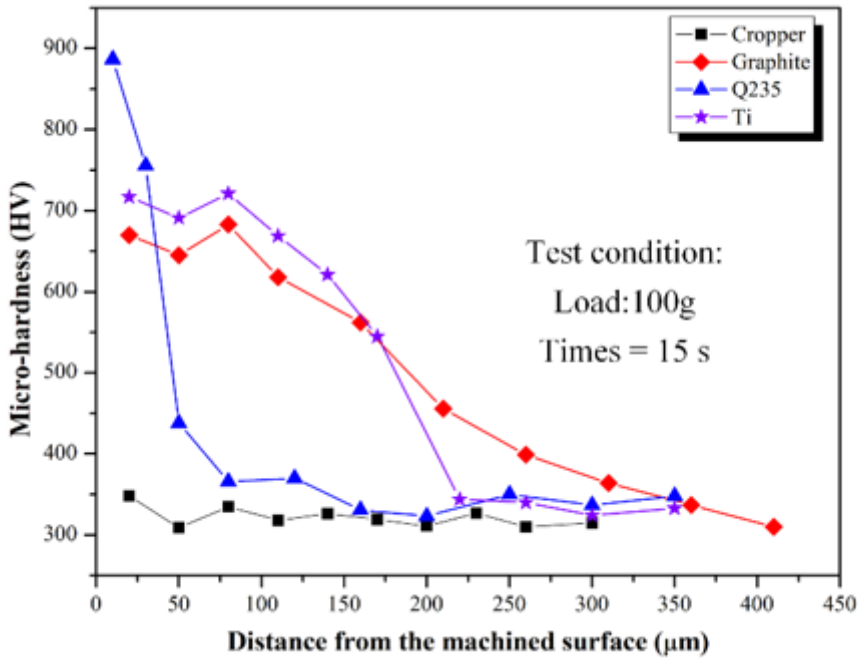

Figure 15

Microhardness of workpiece section prepared using SEAM with different electrodes. (a) Copper, (b) Graphite, (c) Q235 steel and (d) Ti.